Design of Hybrid Position/Force Engagement Controller for Dry Dual Clutch Transmission without Diaphragm Spring

Jiwon J. Oh and Seibum B. Choi

Abstract— This paper suggests a position/force hybrid controller for the dry dual clutch transmission actuators that provides accurate desired clutch normal force tracking performance and also dramatically reduces clutch-transferred torque fluctuation and wheel jerk during vehicle launch and gear shifts when compared to conventional position-based controllers. The proposed controller is composed of a multiple surface sliding mode controller with current estimation for the position-based control and feed-forward clutch normal force controller with clutch normal force estimation for force-based feedback control. Strategy to merge these controllers is suggested for effective actuator control both during the disengaged and engaged phases, which especially serves a significant advantage in clutch control for the system with minimal clutch engagement stroke designed for high actuation efficiency. In order to verify such advantage, the suggested controller is tested on the driveline model for dual clutch transmission and clutch actuators for the clutch system without diaphragm spring that are designed using MATLAB/Simulink. The simulation results reveal that accurate clutch normal force control with reduced jerk is possible even in the absence of the diaphragm spring.

I. INTRODUCTION

While the fuel economy and emission reduction are these days major issues concerning the vehicular technologies, dual clutch transmission has recently been acknowledged as one of the most promising transmission type which may provide high transmission efficiency, fast shift response, seamless torque transmission, and convenience for the driver, all at once. However, dual clutch transmission systems still involve some weaknesses, and one of them is in the use of diaphragm springs.

Because the actuator must push the clutch farther when the diaphragm spring is present, more actuation energy is required to operate the actuator, and the actuation efficiency is degraded. Numerous conventional methods to control clutch actuators are based on position controllers [1-6], and they require diaphragm spring to guarantee the accuracy they claim to provide. The performance of such position-oriented controllers may become degraded due to disturbance such as system wear and thermal expansion [7], especially in the absence of the diaphragm spring with short or nearly no engaged-state clutch stroke.

Thus, in order to attain both control accuracy and actuation efficiency, the proposed algorithm has developed a position/force hybrid controller for the clutch actuators that are capable of directly controlling the clutch normal force

J. J. Oh and S. B. Choi are with Korea Advanced Institute of Science and Technology, 291 Daehak-ro (373-1 Guseong-dong), Yuseong-gu, Daejeon 305-701, Republic of Korea (provide phone: +82-42-350-4120; fax: +82-42-350-4110; e-mail: sbchoi@kaist.ac.kr).

instead of controlling it indirectly through using the empirically predefined position-force relationship stored as a map, and hence eliminates the need for diaphragm springs.

NOMENCLATURE

		Subscript	
ω	speed	e	engine
T	torque	d	damper
J	inertia	c	clutch
α_{th}	throttle angle	t	transfer shaft
θ	angle	o	output
k	torsional stiffness	w	wheel
b	torsional damping coef.	v	vehicle
i_t	transmission gear ratio	1	first clutch side
i_f	final reduction gear ratio	2	second clutch side
i	actuator motor current	m	motor

In addition, all clutches involve disengaged phases with gap between the friction plates, and the characteristics of clutch position and torque variations become completely reversed when passing the kissing point. Although previous works that attempt to reduce the dependency on clutch position exist, they overlook such discontinuous nature of the system and assume near-zero dead zone for the torque increment. Serrarens *et al*. proposed a decoupled engine and clutch approach to control the clutch slip during launch [8], Kim and Choi proposed a vehicle launch controller using a shaft torque observer [9-10], and Tran *et al*. suggested a clutch speed control law based on a Takagi-Sugeno model for dual clutch gear shift [11], but they overlooked the system discontinuity. Langjord *et al*. considered the kissing point, but the controller was largely position-based [12].

Hence in the proposed work, the system discontinuity at the clutch kissing point is realistically considered. By using the position/force hybrid controllers, these two separate controllers and their combined use is shown to be adequate for driver comfort.

II. SYSTEM DESCRIPTION
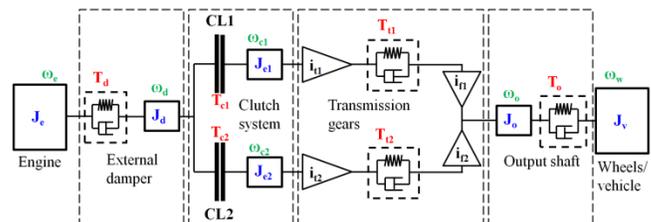
A. Driveline Model

Figure 1. Dual clutch transmission driveline model (J: inertia, T: torque, ω : angular velocity)

For the simulation purpose, a driveline model with dual transfer shaft compliance is developed to reflect realistic internal torque circulation phenomenon that takes place during gear shifts of dual clutch transmissions. The basic structure of the driveline model used is shown in fig. 1.

The following equations listed from (1) to (6) represent the dynamics of each component of the driveline, starting from the engine, external damper, two clutches, output shaft, and wheel.

$$J_e \dot{\omega}_e = T_e - T_d \tag{1}$$

$$J_d \dot{\omega}_d = T_d - T_{c1} - T_{c2} \tag{2}$$

$$J_{e1} \dot{\omega}_{c1} = T_{c1} - \frac{T_{t1}}{i_{t1}} \tag{3}$$

$$J_{e2} \dot{\omega}_{c2} = T_{c2} - \frac{T_{t2}}{i_{t2}} \tag{4}$$

$$J_o \dot{\omega}_o = i_{fi} T_{t1} + i_{fi} T_{t2} - T_o \tag{5}$$

$$J_v \dot{\omega}_w = T_o i_f - T_v \tag{6}$$

Each dynamics involves torque balances, and these torques are modeled as shown next.

$$T_e = f\left(\alpha_{th}, \omega_e\right) \tag{7}$$

Here, the net engine torque is defined as a function of throttle input and engine speed as a map. The external damper torque can be obtained using the known torsional spring and damping constants of the damper.

$$T_d = k_d\left(\theta_e - \theta_d\right) + b_d\left(\omega_e - \omega_d\right) \tag{8}$$

Since the clutch-transferred torques are influenced by different factors depending on whether the clutch is slipping or fully engaged, they must be defined differently according to their states as shown next.

$$T_{c1} = \begin{cases} 0 & \text{, when disengaged} \\ \mu C_{c1} F_{n1} \operatorname{sgn}\left(\omega_d - \omega_{c1}\right) & \text{, when slipping} \\ \dfrac{T_{t1}}{i_{t1}} + J_{e1} \dot{\omega}_{c1} & \text{, when engaged} \end{cases} \tag{9}$$

$$T_{c2} = \begin{cases} 0 & \text{, when disengaged} \\ \mu C_{c2} F_{n2} \operatorname{sgn}\left(\omega_d - \omega_{c2}\right) & \text{, when slipping} \\ \dfrac{T_{t2}}{i_{t2}} + J_{e2} \dot{\omega}_{c2} & \text{, when engaged} \end{cases} \tag{10}$$

Similar to (8), the transfer shaft and output shaft torques are defined using the shaft compliance model.

$$T_{t1} = k_{t1}\left(\frac{\theta_{c1}}{i_{t1}} - i_{f1}\theta_o\right) + b_{t1}\left(\frac{\omega_{c1}}{i_{t1}} - i_{f1}\omega_o\right) \tag{11}$$

$$T_{t2} = k_{t2}\left(\frac{\theta_{c2}}{i_{t2}} - i_{f2}\theta_o\right) + b_{t2}\left(\frac{\omega_{c2}}{i_{t2}} - i_{f2}\omega_o\right) \tag{12}$$

$$T_o = k_o\left(\theta_o - \theta_w\right) + b_o\left(\omega_o - \omega_w\right) \tag{13}$$

Finally, the torque externally lost due to the road gradient, tire rolling resistance, and aerodynamic drag is modeled as shown next.

$$T_v = r_w\left(m_v g \sin\left(\theta_{road}\right) + K_{rr} m_v g \cos\left(\theta_{road}\right) + \frac{1}{2}\rho v_x^2 C_d A\right) \tag{14}$$

Here, r_w, m_v, θ_{road}, K_{rr}, ρ, v_x, C_d, and A denote tire effective radius, vehicle mass, road gradient, rolling resistance coefficient, air density, longitudinal vehicle speed, coefficient of aerodynamic drag, and vehicle frontal area, respectively.

B. Actuator Model

The actuation system considered for the proposed work involves a DC motor with the ball screw mechanism attached to a lever that pushes the clutch disk through a thrust bearing to engage with the engine flywheel side. A simple illustration of the actuator is shown in fig. 2.
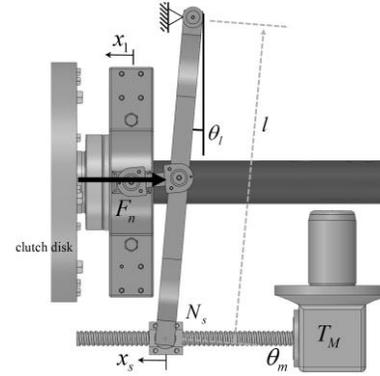

Figure 2. Simplified illustration of the clutch actuator

For simplicity, the lever angle θ_l is assumed negligible, since the clutch stroke is infinitesimal when compared to the lever length l. Also, the equivalent spring constant k_e denotes the combined elasticity of the actuator system, and the equivalent ratio N denotes the quotient of θ_m and x_1 in the absence of motor torque (since the structure of actuator 2 and its controller proposed is analogous to that of actuator 1, all details hereafter are presented only in terms of actuator 1). Here, θ_m represents the motor position after the reduction gear included in the motor assembly.

The clutch normal force is expressed as shown next.

$$F_{n1} = \begin{cases} k_{dia1}\left(x_1 - x_{kiss1}\right), & x_1 \geq x_{kiss1} \\ 0, & \text{otherwise} \end{cases} \tag{15}$$

Here, x_{kiss} denotes the clutch kissing point, which can be identified during the actuator operation [13]. Before the clutch proceeds beyond the kissing point, the clutch is disengaged and no normal reaction force is formed. The clutch normal force begins to form at the kissing point, and increases rapidly. The rate of force increase is affected by the diaphragm spring

constant k_{dia}. Such parameter is required even if the plant does not have a diaphragm spring, since the clutch plate and flywheel structurally acts as a stiff spring. The only difference from the system with diaphragm spring is that the spring constant is considerably higher.

Taking the equivalent actuator spring constant and equivalent actuation ratio into consideration, the relationship between the motor position and the clutch stroke in the presence of the motor torque can be expressed as shown next.

$$x_1 = \frac{1}{N_1}\left(\theta_{m1} - \frac{T_{m1}}{k_{e1}}\right) \tag{16}$$

The mechanical part of the motor dynamics is given next.

$$J_{m1}\ddot{\theta}_{m1} = T_{m1} - T_{fm1} - \frac{F_{n1}}{N_1} \tag{17}$$

where

$$T_{m1} = k_{tq}i_1 \tag{18}$$

Here, i_1 denote the motor current.

The friction torque T_{fm1} is modeled using LuGre friction model and the static Stribeck effect model. Further details can be found in [12]. The electrical dynamic model of the motor is shown as the following.

$$u_1 = R_m i_1 + L_m \frac{di_1}{dt} + V_{emf} \tag{19}$$

where

$$V_{emf} = k_m \dot{\theta}_{m1} \tag{20}$$

The motor parameters k_{tq}, R_m, L_m, and k_m denote motor torque constant, resistance, inductance, and emf constant, respectively.

III. CLUTCH ACTUATOR CONTROLLER

The clutch actuator controller comprises of two major parts: position-based controller and force-based controller. Before the clutch kissing point, the amount of motor position largely changes whereas the normal force stays at zero. On the other hand, beyond the clutch kissing point, the amount of motor position change is minimal while the corresponding normal force change is large, especially in the absence of diaphragm spring. Hence, by controlling either position or force depending on the clutch position, the position/force hybrid controller can provide significant advantage in controlling the clutch stroke and normal force.

A. Position-based Controller

A multiple-surface sliding mode controller is developed for the position controller to be used before the kissing point. A sliding mode controller is considered effective for the system of interest, since accurate position tracking control at the maximum actuator bandwidth can be conveniently achieved with an acceptably simple friction model. Using the first sliding surface, the desired motor current must be

generated. To do so, the motor position tracking error is defined first.

$$\varepsilon_{11} \equiv \theta_{m1} - \theta_{m1d} \tag{21}$$

Using this tracking error, the following sliding surface is formed.

$$\begin{aligned} \dot{s}_{11} &= \ddot{\varepsilon}_{11} + \lambda\dot{\varepsilon}_{11} = \ddot{\theta}_{m1} - \ddot{\theta}_{m1d} + \lambda\dot{\theta}_{m1} - \lambda\dot{\theta}_{m1d} \\ &= \frac{k_{tq}^*}{J_{m1}^*}i_1 - \frac{T_{fm1}^*}{J_{m1}^*} - \frac{\hat{F}_{n1}}{J_{m1}^*N_1} - \ddot{\theta}_{m1d} + \lambda\dot{\theta}_{m1} - \lambda\dot{\theta}_{m1d} \end{aligned} \tag{22}$$

where λ is a positive constant which reflects the actuator bandwidth. The 'hat' on the variable indicates estimated terms, and the superscript '*' indicates nominal models.

$$\text{Let } \dot{s}_{11} = -\eta_{11}sat\left(\frac{s_{11}}{\Phi}\right) \tag{23}$$

and Φ is the smoothing domain for the signum function.

Then we obtain,

$$\begin{aligned} -\eta_{11}sat\left(\frac{s_{11}}{\Phi}\right) &= \frac{k_{tq}^*}{J_{m1}^*}i_1 - \frac{T_{fm1}^*}{J_{m1}^*} - \frac{\hat{F}_{n1}}{J_{m1}^*N_1} \\ &\quad - \ddot{\theta}_{m1d} + \lambda\dot{\theta}_{m1} - \lambda\dot{\theta}_{m1d} \end{aligned} \tag{24}$$

By isolating the current variable, the desired current is computed by the position-based controller as shown next.

$$\begin{aligned} i_{1dp} &= \frac{T_{fm1}^*}{k_{tq}^*} + \frac{\hat{F}_{n1}}{k_{tq}^*N_1} + \frac{J_{m1}^*}{k_{tq}^*}\ddot{\theta}_{m1d} \\ &\quad - \frac{J_{m1}^*\lambda}{k_{tq}^*}\dot{\theta}_{m1} + \frac{J_{m1}^*\lambda}{k_{tq}^*}\dot{\theta}_{m1d} - \frac{J_{m1}^*\eta_{11}}{k_{tq}^*}sat\left(\frac{s_{11}}{\Phi}\right) \end{aligned} \tag{25}$$

To try this result on the actual plant with disturbance, the following is reached.

$$J_{m1}\ddot{\theta}_{m1} = k_{tq}i_{1d} - T_{fm1} - \frac{F_{n1}}{N_1} \tag{26}$$

$$\dot{s}_{11} = -\eta_{11}sat\left(\frac{s_{11}}{\Phi}\right) + \Delta f_{11} + \Delta d_{11} \tag{27}$$

where Δf_{11} and Δd_{11} denote the effects of model uncertainty with the estimation error and disturbance.

Hence, by selecting the gain η_{11} appropriately so that $\dot{s}_{11}s_{11}$ is negative semi-definite, the stability of the system can be shown.

B. Force-based Controller

The force-based clutch actuator controller is composed of both feed-forward and feedback controllers. For the design of the feed-forward controller, the following expression for the motor current can be obtained using the motor dynamics described in (17).

$$i_1 = \frac{J_{m1}\ddot{\theta}_{m1}}{k_{tq}} + \frac{T_{fm1}}{k_{tq}} + \frac{F_{n1}}{k_{tq}N_1} \tag{28}$$

Using the above, the desired motor current can be obtained simply by setting the desired clutch normal force.

$$i_{1df} = \frac{J_{m1}{}^* \dot{\omega}_{m1}}{k_{tq}{}^*} + \frac{T_{fm1}{}^*}{k_{tq}{}^*} + \frac{F_{n1d}}{k_{tq}{}^* N_1} \qquad (29)$$

For the feedback part of the force-based clutch controller, the clutch normal force information is required. However, directly installing the force measurement sensor on the clutch is structurally difficult. Thus an estimation algorithm for the clutch normal force is developed.
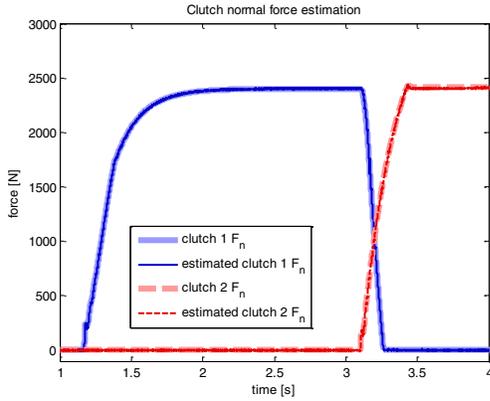

Figure 3. Estimation results for clutch normal forces

Recall the motor dynamics shown in (19). Based on this, the following PI-type unknown input observer can be designed for the purpose of clutch normal force estimation.

$$J_{m1}{}^* \dot{\hat{\omega}}_{m1,obs} = k_{tq}{}^* \hat{i}_{1,obs} - T_{fm1}{}^* - \frac{\hat{F}_{n1}}{N_1} + L_p \left(\omega_{m1} - \hat{\omega}_{m1,obs} \right) \quad (30)$$

$$\hat{F}_{n1} \equiv -L_i N_1 \int \omega_{m1} - \hat{\omega}_{m1,obs} \, dt \qquad (31)$$

$$L_m \dot{\hat{i}}_{1,obs} = -k_m \hat{\omega}_{m1,obs} - R_m \hat{i}_{1,obs} + u_1 \qquad (32)$$

where L_p and L_i are positive tuning parameters for the observer. Here, it is crucial to note that the estimated motor speed and estimated motor current obtained by the normal force observer is exclusively used within the normal force observer only. In other words, these states $-\hat{\omega}_{m1,obs}$ and $\hat{i}_{1,obs}$ — must not be considered identical to $\hat{\omega}_{m1}$ and $\hat{i}_1$ from the current observer that is introduced later.

This observer treats the clutch normal force as an unknown input, while assuming that other terms are identifiable through modeling. When the discrepancy between the model and the actual plant is not negligible, however, the estimator can further be compensated through the actuator compliance shown in (15). With acceptable model uncertainty, accurate estimation of the clutch normal forces can be obtained as shown in fig. 3.

C. Hybrid Control Strategy

As described earlier, the position-based controller and the force-based controller are merged together to form the position-force hybrid controller, so that both clutch stroke and normal force can be controlled effectively.
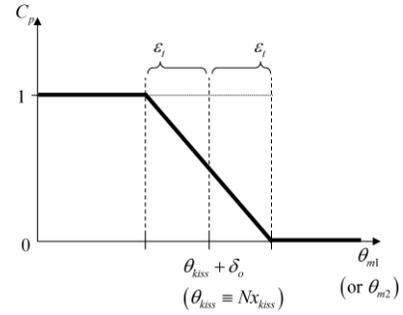

Figure 4. Desired current coefficient generation for hybrid control

Shown in fig. 4 is the strategy to generate coefficients for summing the desired motor currents obtained by the position-based and force-based controllers. Such coefficient is calculated as a function of the motor position relative to the clutch kissing point, as shown next.

$$C_{p1} = sat \left\{ -\frac{1}{2\varepsilon_t} \left(\theta_{m1} - N_1 x_{kiss1} - \delta_o - \varepsilon_t \right) \right\} \qquad (33)$$

Here, δ_o and ε_t are tuning parameters. The coefficient for the clutch 2 is determined in the similar manner.

Note that, so far, two types of desired motor current are defined: position-based desired motor current defined in (25) and force-based desired motor current defined in (29). These are merged using the gain defined in (33) as follows.

$$i_{1d} = C_{p1} i_{1dp} + \left(1 - C_{p1} \right) i_{1df} \qquad (34)$$

Now, for the generation of the motor input, the second sliding surface is defined as the following.

$$s_{12} = i_1 - i_{1d} \qquad (35)$$

With the similar steps exhibited for the first sliding surface formed in the position-based controller, the following equations can be obtained.

$$\dot{s}_{12} = \dot{i}_1 - \dot{i}_{1d} = -\frac{R_m{}^*}{L_m{}^*} i_1 - \frac{k_m{}^*}{L_m{}^*} \dot{\theta}_{m1} + \frac{1}{L_m{}^*} u_1 - \dot{i}_{1d} \qquad (36)$$

$$\text{Let } \dot{s}_{12} = -\eta_{12} sat \left(\frac{s_{12}}{\Phi} \right) \qquad (37)$$

By substituting (37) into (36), we obtain

$$-\eta_{12} sat \left(\frac{s_{12}}{\Phi} \right) = -\frac{R_m{}^*}{L_m{}^*} i_1 - \frac{k_m{}^*}{L_m{}^*} \dot{\theta}_{m1} + \frac{1}{L_m{}^*} u_1 - \dot{i}_{1d} \qquad (38)$$

Now isolating the motor input, the following result is reached.

$$u_1 = L_m{}^* \dot{i}_{1d} + R_m{}^* \hat{i}_1 + k_m{}^* \dot{\theta}_{m1} - L_m{}^* \eta_{12} sat \left(\frac{s_{12}}{\Phi} \right) \qquad (39)$$

Substitution of the input into the system gives the following outcome.

$$\begin{aligned}
& L_m{}^* \dot{i}_{1d} + R_m{}^* \hat{i}_1 + k_m{}^* \dot{\theta}_{m1} - L_m{}^* \eta_{12} sat \left(\frac{s_{12}}{\Phi} \right) \\
& = R_m i_1 + L_m \frac{di_1}{dt} + k_m \dot{\theta}_{m1}
\end{aligned} \qquad (40)$$

$$\dot{s}_{12} = -L_m^{\,*} \eta_{12} \, sat\left(\frac{s_{12}}{\Phi}\right) + \Delta f_{12} + \Delta d_{12} \qquad (41)$$

Hence, again, choosing the η_{12} appropriately so that the feedback term is large enough in magnitude to bound the uncertainty, error, and disturbance guarantees tracking control stability.

Notice that the motor current information is required to obtain the control input. It is replaced by the current estimation obtained by the motor current observer. The current estimation is required and is possible due to the slow bandwidth of the low-power motor. This observer, again, is based on the motor dynamics, shown in the following.

$$\dot{\omega}_{m1} = \frac{k_{tq}}{J_{m1}} i_1 - \frac{T_{fm1}}{J_{m1}} - \frac{F_{n1}}{J_{m1} N_1} \qquad (42)$$

Now, by considering the current as an unknown input, the following observer can be designed.

$$\dot{\hat{\omega}}_{m1} = \frac{k_{tq}^{\,*}}{J_{m1}^{\,*}} \hat{i}_1 - \frac{T_{fm1}^{\,*}}{J_{m1}^{\,*}} - \frac{\hat{F}_{n1}}{J_{m1}^{\,*} N_1} + l_p \left(\omega_{m1} - \hat{\omega}_{m1} \right) \qquad (43)$$

$$\dot{\hat{i}}_1 = l_i \left(\omega_{m1} - \hat{\omega}_{m1} \right) \qquad (44)$$

where l_p and l_i are positive tuning parameters.

IV. SIMULATION

To show the controller performance, simulation using the driveline model with dual clutch transmission with dual transfer shaft compliance is conducted. The main objective of the simulation is to show that, by using the hybrid controller, the accurate tracking ability of the clutch normal force during the steady state, and the reduced wheel jerk and clutch-transferred torque fluctuation can be achieved.

The list of parameters used for the simulation is given next:

Driveline inertia
$J_e = 0.2, J_d = 0.086, J_{e1} = 0.043, J_{e2} = 0.047, J_o = 0.04, J_v = 184.1081$
Driveline shaft spring & damping coefficient
$b_d = 10, k_{t1} = 15420, b_{t1} = 53, k_{t2} = 14980, b_{t2} = 51, k_o = 9520, b_o = 591$
Gear ratio
$i_{t1} = 3.688, i_{t2} = 2.85, i_{f1} = i_{f2} = 4.647$
Vehicle specification
$r_w = 0.338, m_v = 1596, \theta_{road} = 0, K_{rr} = 0.015, \rho = 1.225, C_d = 0.325, A = 2.2126$
Clutch & actuator specification
$\mu = 0.27, C_{c1} = 0.21, C_{c2} = 0.1684, k_{dia} = 7 \times 10^6, x_{kiss} = 0.002, N = 88.7,$
$k_e = 6 \times 10^6, J_m = 0.0165, k_{tq} = 0.8593, R_m = 0.2536, L_m = 0.0575, k_m = 0.8593$
Controller gains
$\lambda = 75, \Phi = 0.01, \eta_{11} = \eta_{21} = 1500, \eta_{12} = \eta_{22} = 10, L_p = 100, L_i = 5000, l_p = 500,$
$l_i = 30000, \varepsilon_r = 0.02, \delta_o = 0$ [units are SI derived (kg, m, s, A)]

Three different controllers are involved in the simulation. The position-based controller attempts to raise the motor position to the point which corresponds to the desired force according to the position-force map as accurately and rapidly as possible. The position profile-based controller – the most common form of controller used in conventional clutch actuator controller design – operates similarly, but the desired position takes the form of a predefined optimized profile shape instead of a simple step function. This profile was determined

by trial and error to minimize the clutch jerk. Finally, the hybrid controller operates according to the control strategy introduced in the proposed work.

Since the motor actuators are chosen to operate on vehicle, the motor inputs shown in fig. 5 are bounded between -12V and 12V. These input signals reveal that the input signals generated by the hybrid controllers effectively attempt to decelerate the clutch engagement just around the kissing point so that the impact on the clutch can be minimized. This can be seen more clearly when the motor position control result displayed in fig. 6 is observed.
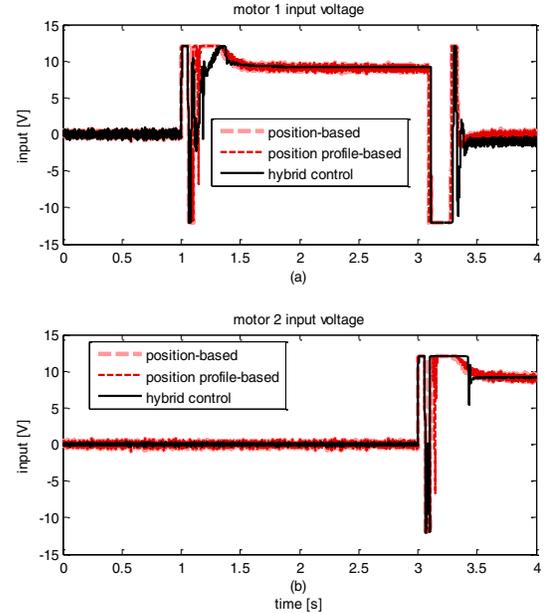
Figure 5. Plot of actuator input voltage during launch and gear shift: (a) for actuator 1, (b) for actuator 2
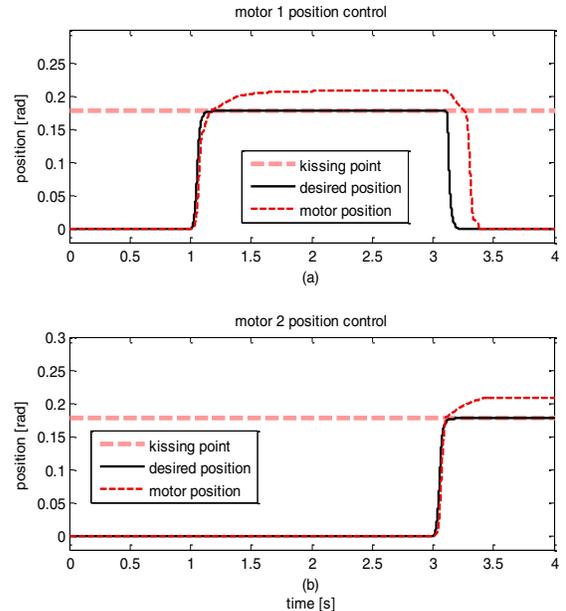
Figure 6. Plot of actuator motor position tracking control result during launch and gear shift: (a) for actuator 1, (b) for actuator 2

As shown in fig. 6, before reaching the kissing point, the hybrid controller puts more emphasis on the position-based control, which causes the motor position to track the desired position accurately. This naturally leads to deceleration of the motor near the kissing point to avoid overshoot. Then soon the force-based controller completely takes over and takes the clutch stroke beyond the kissing point so that the actuators operate following the desired force instead of desired positions.
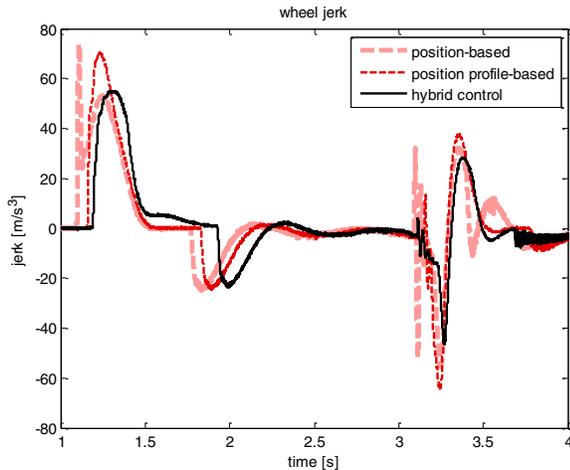

Figure 7.   Plot of wheel jerks obtained using different controllers during launch and gear shift (low pass filtered for improved visibility)

TABLE I.   QUANTITATIVE RESULT OF WHEEL JERK

Controller type	Launch		Gear shift	
	Magnitude of max jerk [m/s^3]	% change	Magnitude of max jerk [m/s^3]	% change
Position -based	73.87	baseline	64.45	baseline
Position profile-based	70.60	-4.43%	55.47	-13.93%
Hybrid controller	55.18	-25.30%	46.5	-27.85%

The aforementioned differences in outcome among the cases of using different controllers are reflected in the wheel jerk, which is shown in fig. 7. Here, it can be seen that, at the cost of an acceptable amount of delay in driveline response – which is inevitable, since the actuator must decelerate to reduce clutch impact – the hybrid controller achieves minimum wheel jerk response among all controllers. The wheel jerk reduction by hybrid control is quantitatively dealt in table 1.

V.   CONCLUSION

This study has proposed a novel strategy to control the DC motor actuators for the dual clutch transmission with omitted diaphragm spring. Making use of only the information already available in typical production vehicles with the dual clutch transmission, effective clutch actuator control algorithms are developed. Summarizing the paper, three noteworthy contributions found in the suggested work are the following: tracking control ability of the clutch normal force even for systems without diaphragm spring, considerable

reduction of wheel jerk and backward torque recirculation phenomenon, and hybrid control method enabled by costless design of clutch normal force estimator. The work shall be further extended to develop a clutch normal force estimator which also utilizes the actuator compliance model for improved robustness, and a clutch transferred torque-based controller that is robust against clutch friction coefficient uncertainty.

REFERENCES

[1] J. Horn, J. Bamberger, P. Michau, S. Pindl, "Flatness-based clutch control for automated manual transmissions," Control Engineering Practice, vol 11, no. 12, pp. 1353-1359, 2003
[2] J. Deur, V. Ivanović, Z. Herold, M. Kostelac, and H. E. Tseng, "Dry clutch control based on electromechanical actuator position feedback loop". International Journal of Vehicle Design, vol. 60, no. 3, pp. 305-326, 2012.
[3] J. Kim, S. B. Choi, H. Lee, J.Kang, and M. Hur, "System Modeling and Control of a Clutch Actuator System for Dual Clutch Transmissions" in KSAE Annual Conference & Exhibition, 2011, pp. 1253-1257.
[4] J. Kim, S. B. Choi, H. Lee, J. Koh, "Design of a robust internal-loop compensator of clutch positioning systems," in 2012 IEEE International Conference on Control Applications (CCA), 2012, 1473-1478.
[5] F. Vasca, L. Iannelli, A. Senatore. G. Reale, "Torque transmissibility assessment for automotive dry-clutch engagement," IEEE/ASME Transactions on Mechatronics, vol. 16, no. 3, pp. 564-573, 2011
[6] C. Dragos, S. Preitl, R. Precup, E. M. Petriu, A. Stinean, "Adaptive control solutions for the position control of electromagnetic actuated clutch systems," in Intelligent Vehicles Symposium (IV), 2012, pp. 81-86.
[7] A. Myklebust, L. Eriksson, "The Effect of Thermal Expansion in a Dry Clutch on Launch Control," 7th IFAC Symposium on Advances in Automotive Control, 2013.
[8] A. Serrarens, M. Dassen, M. Steinbuch, "Simulation and control of an automotive dry clutch," in Proceedings of the 2004 American Control Conference, 2004, vol. 5, pp. 4078-4083.
[9] J. Kim, S.B. Choi, "Control of dry clutch engagement for vehicle launches via a shaft torque observer," in American Control Conference (ACC), 2010, pp. 676-681.
[10] J. Kim, K. Choi, S.B. Choi, " Gear shift control of Dual Clutch Transmissions with a torque rate limitation trajectory," in American Control Conference (ACC), 2011, pp. 3338-3343.
[11] V. N. Tran, J. Lauber, M. Dambrine, "H∞ gearshift control of a dual clutch based on uncertain TS models," in American Control Conference (ACC), 2013, pp. 4891-4896.
[12] H. Langjord, G. O. Kaasa, T. A. Johansen, "Adaptive observer-based switched control for electropneumatic clutch actuator with position sensor," World Congress, vol. 18, no. 1, pp. 4791-4796, 2011.
[13] J. Oh, S. B. Choi, "Design of Dry Dual Clutch Transmission Actuator Controller for Simultaneous Kissing Point Identification Using Multiple Sliding Surfaces," in 13th International Conference on Control, Automation and Systems, 2013.